A NUMERICAL STUDY FOR COATING OF VENTILATION DUCTS USING JET INJECTION

by

Cihan SEZER[a*], Kenan KAYA[a], Busra Selenay ONAL[a], Hasan Alpay HEPERKAN[a], and Oktay OZCAN[b]

[a] Department of Mechanical Engineering, Faculty of Engineering, Istanbul Aydin University, Kucukcekmece, Istanbul, Turkey
[b] Department of Aeronautical Engineering, Faculty of Engineering and Architecture, Istanbul Gelisim University, Avcilar, Istanbul, Turkey

Original scientific paper
https://doi.org/10.2298/TSCI221230119S

In this study, the performance of a novel method where an antibacterial solution is pressurized and sprayed into recirculated air through nozzles, is investigated numerically. This resembles a jet in a cross-flow problem where the antibacterial solution mixes with ventilation air and further adheres to the inner surfaces of the duct. The motion of particles dispersed in antibacterial solution is described as the advection of a passive scalar, i.e., temperature, allowing for a single-phase flow solution. The effectiveness of the coating is evaluated by the temperature distribution on the inner surfaces of the duct. Single phase 3-D turbulent flow of air at two different temperatures is modeled and the velocity and temperature fields in the ventilation duct were calculated using the commercial code ANSYS FLUENT. The numerical model is validated by experiments conducted on a full-scale test rig, in terms of temperature. The numerical calculations were conducted in four series: where the effect of the nozzle arrangement, the jet injection angle, the jet-to-cross-flow velocity ratio, and a time-dependent jet velocity profile of a sinusoidal wave form are investigated. The numerical solutions show that the coating is highly inefficient for velocity ratios less than 3.3, and the period of time-varying jet stream has little effect on the coating performance.

Key words*: antibacterial coating, indoor air quality, jet in cross-flow, temperature measurement, computational fluid dynamics*

Introduction

Air quality in ventilation systems, particularly those installed in crowded places such as hospitals, shopping malls and schools, is a critical issue regarding the human health. The HVAC units and air ducts are prone to pathogens such as mold, fungus, and other microbial contaminants as they easily accumulate and reproduce, endangering the human health. Such a contamination also decreases the performance of a ventilation system and increases its energy consumption.

Cleaning the HVAC unit and duct system regularly is one approach to keep the indoor air quality at an acceptable level. There are three different conventional methods for cleaning air ducts: contact method, air sweeping method, and rotary brush method [1]. Another method involves spraying a volatile liquid containing the antibacterial substance through the duct inlet.

* Corresponding author, e-mail: cihansezer@aydin.edu.tr

As the solvent evaporates, a dry film layer of polymer-supported antibacterial agent forms on the duct walls, preventing the formation of a suitable environment for fungi and bacteria [2]. In this method, antibacterial substance or sealant is sprayed into the duct inlet, so that it is carried along the duct with the air-flow. However, according to the North American Insulation Manufacturers Association (NAIMA) report [3], the tests performed for this method indicate that the antibacterial solution cannot effectively cover all surfaces of the duct. The numerical study by Wang *et al.* [4], who report that particles of various sizes in a rectangular channel tend to accumulate in the corner regions of the channel, justifies this observation.

This study investigates the effectiveness of a novel method of duct coating, where antibacterial aerosol is sprayed into the ventilation air as a jet stream rather than through the duct inlet. This is a basic fluid mechanics problem known as jet in cross-flow (JICF), on which there are many experimental [5-13] and computational [13-19] studies. Meyer *et al.* [6] and Ozcan and Larsen [7] present particle image velocimetry and laser doppler anemometry data obtained in a wind tunnel at velocity ratios of 3.3 and 1.3. Meyer *et al.* [8] present results of a proper orthogonal decomposition analysis which identifies the vortical structures in the flow field. Kamotani and Greber [9] report mean velocity and turbulence data obtained by thermal anemometry in a water channel at velocity ratios of 2, 4, and 6.

Smith and Mungal [10] employ experimentally obtained data to discuss the mixing characteristics of an air jet seeded with acetone vapor and injected into an air cross-flow at various velocity ratios between 5-200. Ryan *et al.* [11] present experimental and computational data obtained by large eddy simulation (LES) for the velocity and concentration fields of an inclined jet injected into a water channel. Ivanova *et al.* [12] present computational results obtained by the RANS and LES to determine turbulent Schmidt number for a normal JICF. According to their findings, the outcomes obtained via LES are better than those by RANS. Galeazzo *et al.* [13] present experimental and numerical data for the velocity and concentration fields of a normal JICF. They compare the numerical results from RANS and LES to experimental data. They conclude that unlike the results of the RANS model, data obtained by the LES calculations agree well with their experimental data.

A computational study of Karvinen and Ahlstedt [14] compare turbulence models of standard k-ε, k-ε RNG, standard k-ω, and SST k-ω, for a jet-to-cross-flow velocity ratio of 3.3. Demuren [15] employs the Reynolds stress equation model to study turbulence characteristics of a round JICF at velocity ratios of 0.5 and 2.0. Keimasi and Taeibi-Rahni [16] and Hoda and Acharya [17] present computational data to evaluate accuracy of various eddy-viscosity based models for a square jet injected vertically into a cross-flow. They observe that the standard k-ω and k-ε RNG turbulence models provide unrealistic velocity profiles, whereas SST k-ω and standard k-ε yield the most satisfactory results. Kalita *et al.* [18] and Huang *et al.* [19] report computational results obtained by using eddy-viscosity based turbulence models for 2-D JICF.

Coletti *et al.* [20] present experimental and computational data for a liquid inclined jet injected into a water tunnel at the velocity ratio of one. Herrmann [21] presents computationally obtained concentration data to discuss the atomization of a liquid jet injected into a gaseous cross-flow at the velocity ratio of 6.6. Chang *et al.* [22] report the results of a numerical study in case of constant and pulsating 2-D jets for velocity ratios between 1-4. Sau and Mahesh [23] perform direct numerical simulations to investigate the mixing behavior of pulsating jet and present optimal parameters for the velocity ratio and jet-stream period. Kartaev *et al.* [24] present experimental and computational data for multiple jets injected radially into a cylindrical channel.

In this study, a novel coating method, that is, the jet injection method, for ventilation ducts is proposed and the results of numerical calculations to evaluate the effectiveness of the proposed method are presented for a duct of a square cross-section. Four series of numerical calculations are performed: effect of the arrangement of nozzles, and jet injection angle on the temperature distribution is investigated in the first and second series, respectively, while the effect of jet-to-cross-flow velocity ratio is investigated in the third series. The fourth series considers the case of a jet stream with time-dependent mean velocity with a sinusoidal profile, where various periods are considered. It is assumed that the motion of the particles dispersed in antibacterial solution can numerically be modeled as advection of a passive scalar, *i.e.*, temperature, allowing a single-phase flow solution, which can be valid if particles injected into air have a low Stokes number.

Numerical method

The commercial CFD solver, ANSYS FLUENT is employed for the numerical calculations, where the discretized form of the incompressible, 3-D RANS equations, *i.e.*, the continuity, momentum and energy equations are solved, which are given:

$$\frac{\partial u}{\partial x}+\frac{\partial v}{\partial y}+\frac{\partial w}{\partial z}=0 \tag{1a}$$

$$\rho\left[\frac{\partial u}{\partial t}+u\frac{\partial u}{\partial x}+v\frac{\partial u}{\partial y}+w\frac{\partial u}{\partial z}\right]=-\frac{\partial p}{\partial x}+\mu\left(\frac{\partial^2 u}{\partial x^2}+\frac{\partial^2 u}{\partial y^2}+\frac{\partial^2 u}{\partial z^2}\right) \tag{1b}$$

$$\rho\left[\frac{\partial v}{\partial t}+u\frac{\partial v}{\partial x}+v\frac{\partial v}{\partial y}+w\frac{\partial v}{\partial z}\right]=-\frac{\partial p}{\partial y}+\mu\left(\frac{\partial^2 v}{\partial x^2}+\frac{\partial^2 v}{\partial y^2}+\frac{\partial^2 v}{\partial z^2}\right) \tag{1c}$$

$$\rho\left[\frac{\partial w}{\partial t}+u\frac{\partial w}{\partial x}+v\frac{\partial w}{\partial y}+w\frac{\partial w}{\partial z}\right]=-\frac{\partial p}{\partial z}+\mu\left(\frac{\partial^2 w}{\partial x^2}+\frac{\partial^2 w}{\partial y^2}+\frac{\partial^2 w}{\partial z^2}\right) \tag{1d}$$

$$\rho c_p\left[\frac{\partial T}{\partial t}+u\frac{\partial T}{\partial x}+v\frac{\partial T}{\partial y}+w\frac{\partial T}{\partial z}\right]=k\left(\frac{\partial^2 T}{\partial x^2}+\frac{\partial^2 T}{\partial y^2}+\frac{\partial^2 T}{\partial z^2}\right) \tag{1e}$$

where u, v, and w [ms^{-1}], and x, y, and z [m] are the velocity components and the spatial co-ordinates in the Cartesian co-ordinate system, respectively, T [K] and t [s] – the temperature and time, while ρ [kg/m^3], μ [kgm^{-1}s^{-1}], c_p [Jkg^{-1}K^{-1}], and k [Wm^{-1}K^{-1}] – the density, dynamic viscosity, specific heat, and thermal conductivity of air, respectively. In this work incompressible, 3-D steady RANS equations are solved for the first three series, while unsteady formulation is employed for the fourth series. Properties of air *i.e.* density, viscosity, specific heat, and thermal conductivity, are assumed to be constant. The unsteady RANS equations given by eq. (1) are for constant-property flow, whereas the time-derivative terms are dropped for steady cases. The energy equation is also solved since it is assumed that particles injected into the cross-flow have an insignificant Stokes number, allowing the concentration field of the antimicrobial solution be represented by a passive scalar such as temperature, in a single-phase flow.

For modelling turbulence, k-ω SST turbulence model, *i.e.*, a two-equation RANS model is given [25]:

$$\frac{\partial}{\partial t}(\rho k)+\frac{\partial}{\partial x_i}(\rho k u_i)=\frac{\partial}{\partial x_j}\left(\Gamma_k\frac{\partial k}{\partial x_j}\right)+G_k-Y_k \tag{2a}$$

$$\frac{\partial}{\partial t}(\rho\omega)+\frac{\partial}{\partial x_i}(\rho\omega u_i)=\frac{\partial}{\partial x_j}\left(\Gamma_\omega\frac{\partial\omega}{\partial x_j}\right)+G_\omega-Y_\omega+D_\omega \tag{2b}$$

where k [m^{2}s^{-2}] and ω [s^{-1}] are the specific turbulence kinetic energy and specific turbulence dissipation rate, respectively. The terms Γ, G, and Y indicate effective diffusivity, production, and dissipation of the corresponding quantity, respectively, while D_ω represents the cross-diffusion modification term which appears due to blending the standard k-ω and the standard k-ε models together. The SIMPLE algorithm for pressure-velocity coupling is used, while the convective terms in the momentum and energy equations are discretized using a second order upwind interpolation scheme. Second order discretization scheme is employed for diffusion and pressure terms.

The solution domain has a height, H, and length, L, of 150 mm and 2000 mm, respectively, while it has only half-width (W/2) of the actual duct, *i.e.* 75 mm, since the mean flow and time-averaged turbulent structures are assumed to be symmetrical about the longitudinal vertical mid-plane, fig. 1(a). The nozzle diameter is D = 20 mm, and the nozzles are located 3D downstream of the duct inlet, while they are equally spaced in the spanwise direction. An unstructured grid of 1.2 million hexahedral prism elements is generated, fig. 1(b), while elements of relatively smaller size are created adjacent to the wall. The boundary conditions are also illustrated in fig. 1(a). The velocity inlet boundary condition is applied at cross-flow and jet inlet, where uniform velocity and temperature profiles are defined. The inlet temperature of the cross-flow and jet stream is T_C = 293 K and T_j = 313 K, respectively, for all cases. Duct exit is modeled by the pressure outlet condition, where static pressure is fixed at zero gauge.

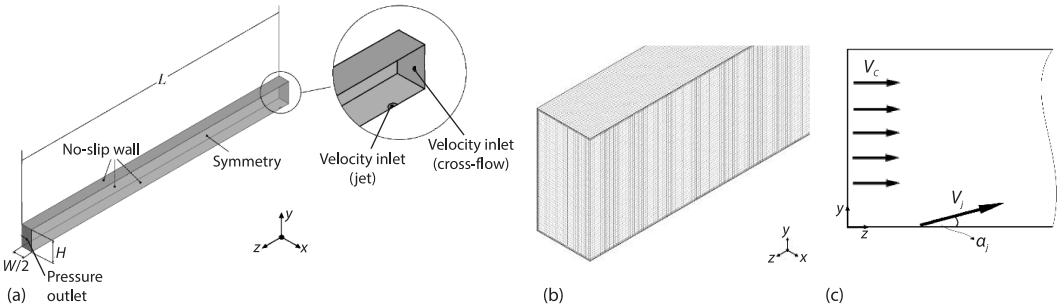

Figure 1. A general view of (a) the solution domain with some geometric parameters and applied boundary conditions, (b) the grid used in calculations, and (c) the definition of cross-flow and jet velocities (V_c and V_j), and jet injection angle (α_j)

Symmetry condition is assigned to the vertical mid-plane, while the duct walls are defined as no-slip walls. Definitions of jet injection angle, as well as cross-flow and jet velocities, V_c and, V_j, respectively, are schematically shown in fig. 1(c).

The percentage area of the inner surfaces wetted by the jet stream is regarded as the main criterion for assessing the effectiveness of a single case. For this purpose, temperature distribution on the inner surfaces of the duct is evaluated by introducing a dimensionless parameter, θ, which normalizes the temperature data into the interval 0 and 1:

$$\theta_i=\frac{T_i-T_c}{T_j-T_c} \tag{3}$$

where T_i is the temperature of a selected node on the inner surface of the duct. A value of θ_i = 1.0 corresponds to the jet temperature, whereas θ_i = 0 indicates the pure cross-flow. A us-

er-defined function is implemented into the solver to calculate the areal distribution of dimensionless temperature, θ, on the inner surface of the duct. Accordingly, range of θ is uniformly divided to five discrete zones, and percentage of their corresponding surface areas are identified, tab. 1. Coating efficiency is determined considering the area percentage of the distinct temperature zones, where $A_{\mathrm{I}} = 100$ and $A_{\mathrm{V}} = 100$ correspond to two extrema, that is, the worst and the ideal cases, respectively.

Table 1. Temperature zones and their corresponding areas on the inner surfaces of the duct

Temperature zone	Range of θ	Percentage area of temperature zone [%]
θ_{I}	$0.0 \le \theta < 0.2$	A_{I}
θ_{II}	$0.2 \le \theta < 0.4$	A_{II}
θ_{III}	$0.4 \le \theta < 0.6$	A_{III}
θ_{IV}	$0.6 \le \theta < 0.8$	A_{IV}
θ_{V}	$0.8 \le \theta \le 1.0$	A_{V}

In a JICF problem, velocity ratio, V_R, is defined as the ratio of the jet velocity, V_j, to that of the cross-flow, V_{c}, as given:

$$V_R = \frac{V_{\mathrm{j}}}{V_{\mathrm{c}}} \tag{4}$$

A mesh independence study is performed with coarse and fine grid configurations, while the maximum values of y^+, which is defined by $u_\tau y/\mu$, are 14.63 and 10.22, respectively, tab. 2. Accordingly, the normalized root mean square error in percentage area of temperature zones is less than 2%. Therefore, the fine mesh configuration with approximately $8 \cdot 10^5$ elements is used.

Table 2. Results of the mesh independence study

Case	Number of elements	Maximum y^+	A_{I} [%]	A_{II} [%]	A_{III} [%]	A_{IV} [%]	A_{V} [%]
Coarse	$3 \cdot 10^5$	14.63	26.63	63.57	5.85	3.35	0.61
Fine	$8 \cdot 10^5$	10.22	25.82	63.92	4.54	4.77	0.95

Validation

A test rig is installed to validate the numerical method, which consists of an air duct of 5 m length and 0.15 m × 0.15 m rectangular cross-section, fig. 2. An axial fan generates the cross-flow, which passes through an adapter and enters the channel. The jet stream is fed into the channel via PVC pipes which are connected to the collector tank where air supplied by the radial fan is heated. Temperature is measured with *T*-type thermocouples connected to a data logger, at two different cross-sections, that is, C1 and C2, fig. 2(a), which are 1.4 m and 1.7 m downstream of the inlet, respectively. There are three slots at each cross-section, which are coincident with the longitudinal center axis of the side and top surfaces of the duct. Thermocouples are flush against the duct walls, so that temperature of the inner surface can be measured. The uncertainty of the temperature measurements is ±1 °C. The inlet velocity of the cross-flow and jet stream is controlled by frequency inverters connected to the fans, while the values of

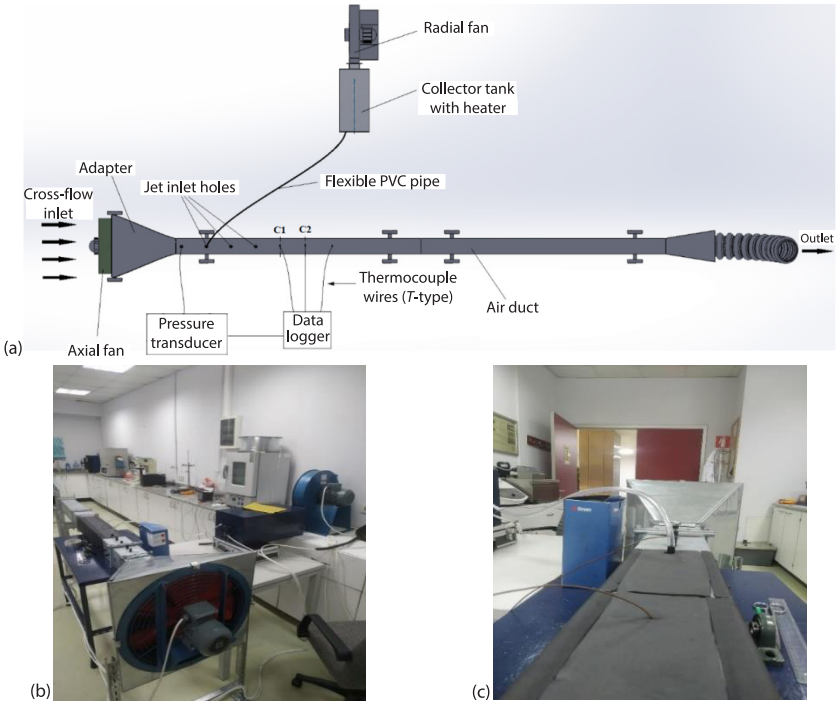

Figure 2. (a) A schematic illustration, and (b), (c) photos of the test rig

inlet velocity values are obtained by measuring the average inlet pressure of the cross-flow and jet stream. The average pressure of the cross-flow is measured using a differential pressure transducer, while that of the jet-stream is measured by a Pitot tube connected to a *U*-tube manometer. Inlet velocities of $V_c = 3$ m/s and $V_j = 9$ m/s are considered in the experiments, which yield a velocity ratio of $V_R = 3$. The inlet temperatures of the cross-flow and jet stream are measured as $T_j = 300.6$ K and $T_c = 314.7$ K, respectively. Table 3 presents cross-sectional average values of surface temperature at specified locations obtained experimentally and numerically. Accordingly, absolute value of the deviation between the numerical and experimental results, which is normalized by the maximum temperature difference throughout the system (*i.e.*, $T_j - T_i$) is less than 3%, which is larger than the uncertainty in temperature measurement. Thus, it is concluded that the numerical set-up employed in this study is validated and can reliably be used for estimating the temperature field.

Table 3. Comparison of the experimental and numerical results

Location	Distance from inlet [m]	Temperature [K]		Absolute value of the normalized error [%]
		Experimental	Numerical	
C1	1.4	301.2	300.9	1.98%
C2	1.7	301.5	301.1	2.84%

Results and discussion

First series: effect of the nozzle arrangement

The first series of calculations are conducted to investigate the effect of the nozzle arrangement by numerical simulations. For this purpose, four geometrical models having different nozzle arrangements, fig. 3, are compared for an injection angle of $\alpha_j = 90°$ and velocity ratio of $V_R = 3.3$. Cross-flow and jet stream enter the domain at temperatures of 293 K and 313 K, respectively, while the Reynolds number, based on the cross-flow velocity and hydraulic diameter of the channel, is 30800. Jet-to-cross-flow velocity ratio, V_R is also constant and kept at 3.3.

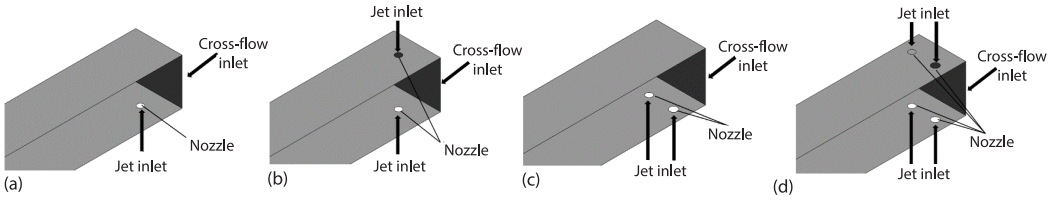

Figure 3. Illustration of the geometrical models of the physical domain of the problem and corresponding nozzle arrangements for; (a) Case I-a, (b) Case I-b, (c) Case I-c, and (d) Case I-d

Figure 4 shows the temperature zones and their distribution on the inner surfaces of the duct, for the first series of calculations, where a positive trend indicates a better contact between the jet and cross-flow mixture, and the wall. Considering the results related to Cases I-b and I-c, it can be concluded that it is the existence of the opposite jets, rather than mass-flow rate of the jet, which enhances the spreading of the passively advected agent, in this case, temperature, on the inner walls, figs. 4(b) and 4(c). Similarly, the advantage of Case I-d over Case I-b cannot be explained only by its higher overall flow rate of jets, hence the geometrical model of Case I-d is employed for the second series of calculations.

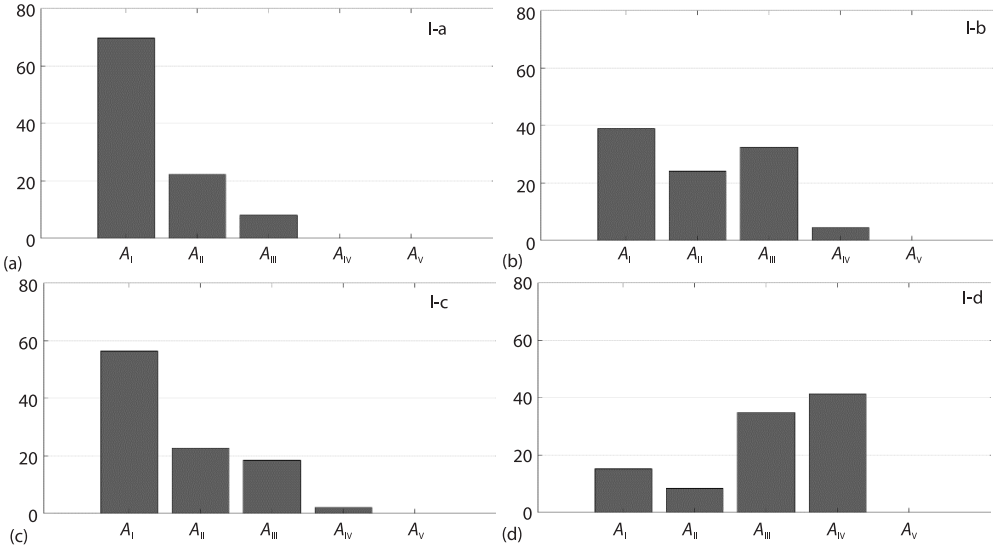

Figure 4. Percentage areas corresponding to each temperature zone for the first series of calculations

Second series: effect of the jet injection angle

In the second series of numerical calculations, effect of the jet injection angle, α_j, is investigated using the geometrical model of Case I-d, fig. 3(d), by keeping $V_R = 3.3$, and the Reynolds number the same as in the first series.

In tab. 4, values of the percentage area of each temperature zone related to the second series of calculations are tabulated. Note that cases with a relatively smaller value of A_I as well as a larger value of A_{IV} are favorable. Thus, it can be deduced that, configurations with injection angles of 75° and 90° both yield the best performance for coating of the wall. The A_I is the smallest for $\alpha_j = 135°$, however it has the smallest value of A_{IV} as well, among the cases. The most homogenous distribution of temperature zones is achieved for $\alpha_j = 105°$, as it has the smallest standard deviation. An interesting result is that the distributions are nearly the same with the jet injection angles of 60°, and 120° which does not apply for the other symmetrical pairs of angles. Generally, a weak interaction between opposing jet streams injected from the bottom and top surfaces of the duct leads to an undesirable temperature distribution.

Table 4. Percentage area of temperature zones for the second series of calculations

Case	Jet injection angle, α_j	A_I	A_{II}	A_{III}	A_{IV}	A_V
II-a	45°	36.22	23.92	33.22	6.62	0.00
II-b	60°	23.49	24.86	20.97	30.66	0.00
II-c	75°	15.49	8.57	37.87	35.14	2.91
II-d	90°	15.29	8.42	34.95	41.31	0.03
II-e	105°	23.92	14.25	28.96	27.62	5.25
II-f	120°	22.44	24.14	23.45	29.94	0.01
II-g	135°	13.52	56.75	25.26	4.20	0.07

Because the vertical component of the jet stream momentum is reduced, this could explain why the cases with injection angles far below or above 90° work rather smaller.

Third series: effect of the velocity ratio

The effect of the velocity ratio, V_R, is investigated in the third series numerical calculations for $V_R = 0.5$, 1, 2, 3.3, 4, 6, and 8. While the geometry of Case I-a, fig. 3(a), is adopted. Values of the parameters considered in the third series of the numerical calculations are presented in tab. 5.

Table 5. Parameters used in the third series of numerical calculations

Case	T_c [K]	V_c [ms^{-1}]	T_j [K]	V_j [ms^{-1}]	V_R
III-a	293	3.0	313	1.5	0.5
III-b				3.0	1
III-c				6.0	2
III-d				10.0	3.3
III-e				12.0	4
III-f				18.0	6
III-g				24.0	8

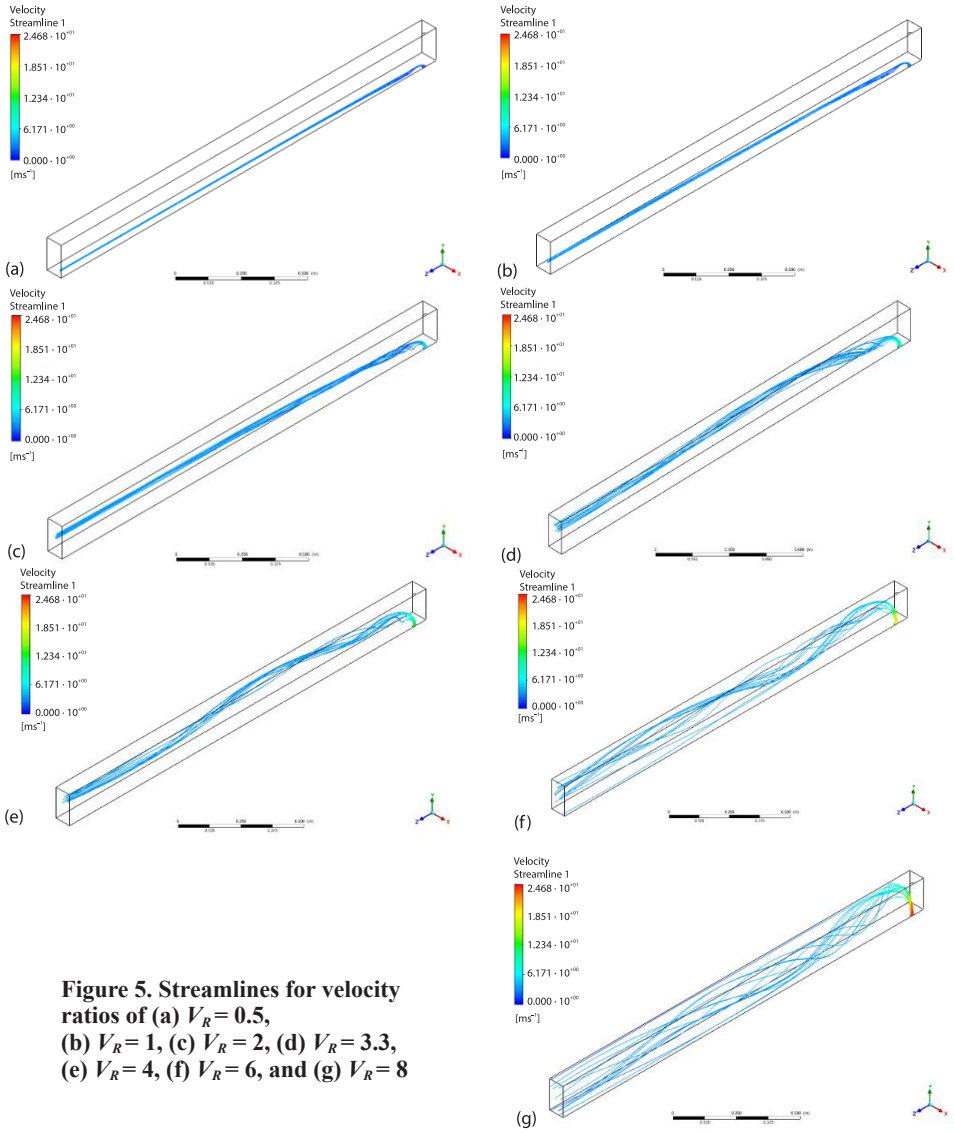

Figure 5. Streamlines for velocity ratios of (a) V_R = 0.5, (b) V_R = 1, (c) V_R = 2, (d) V_R = 3.3, (e) V_R = 4, (f) V_R = 6, and (g) V_R = 8

Table 6 shows the results of the third series of calculations, where it is seen that almost the whole inner surface of the air duct remains in the lowest temperature zone for the cases III-a, III-b, and III-c, for velocity ratios of V_R = 0.5, 1, and 2, respectively, which indicates that the inner surface cannot be coated efficiently. However, the percentage area corresponding to the lowest temperature zone, A_1, starts decreasing with velocity ratio beyond V_R = 3.3. The 3-D streamlines and temperature contours on the duct walls are presented in figs. 5 and 6, where the enhancement in coating efficiency can be observed. Accordingly, increase in interaction between the jet stream and inner surfaces of the duct is evident, which is caused by larger-momentum impact between the jet stream and the top wall.

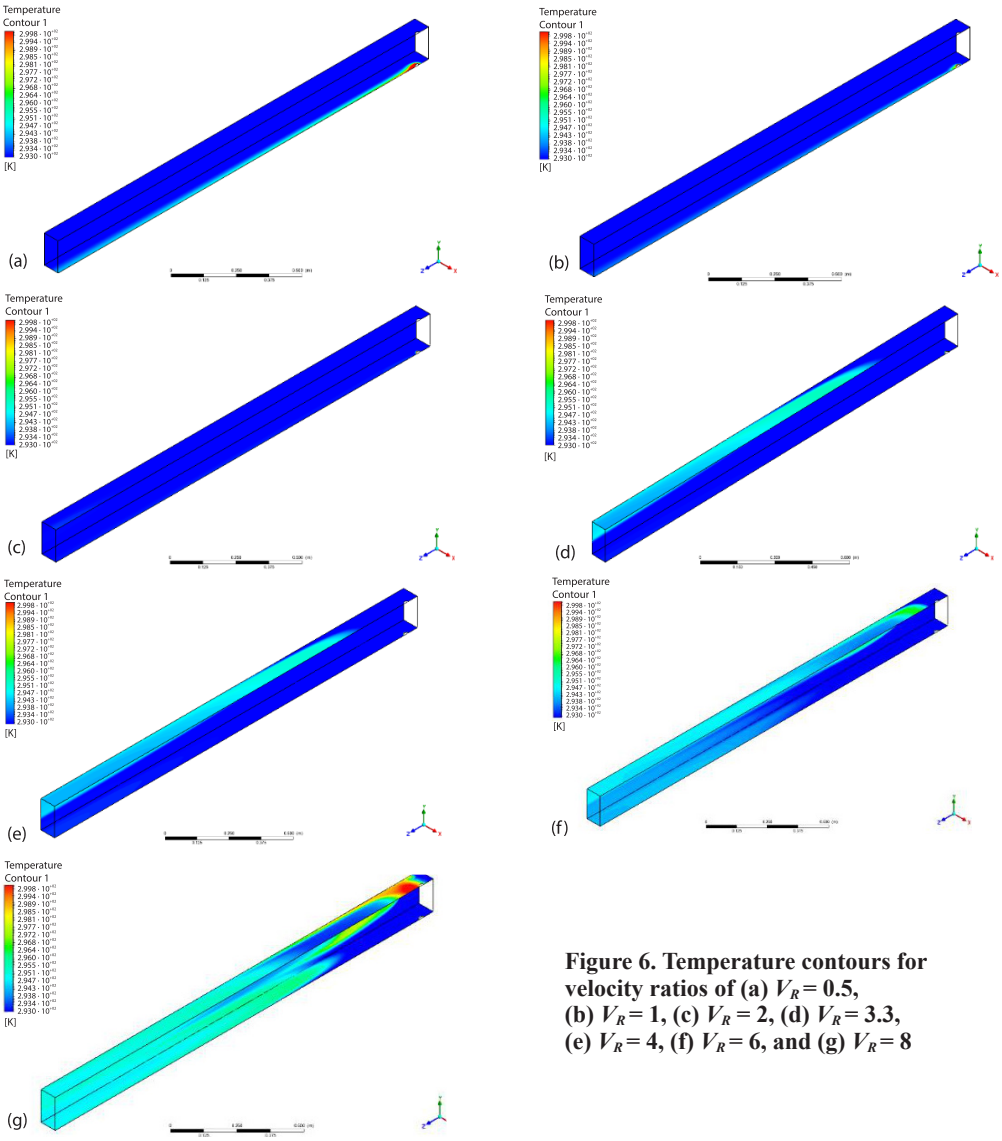

Figure 6. Temperature contours for velocity ratios of (a) $V_R = 0.5$, (b) $V_R = 1$, (c) $V_R = 2$, (d) $V_R = 3.3$, (e) $V_R = 4$, (f) $V_R = 6$, and (g) $V_R = 8$

Table 6. Results related to the third series of calculations

Case	A_I [%]	A_{II} [%]	A_{III} [%]	A_{IV} [%]	A_V [%]
III-a	99.63	0.27	0.05	0.04	0.00
III-b	99.88	0.09	0.02	0.01	0.01
III-c	99.98	0.01	0.00	0.01	0.00
III-d	72.88	22.50	7.70	0.00	0.00
III-e	61.60	1.87	7.70	17.18	11.64
III-f	29.72	33.99	32.00	3.04	1.25
III-g	25.82	63.92	4.54	4.77	0.95

Fourth series: effect of the pulsative jet inlet

In the fourth series of calculations, a time-dependent sinusoidal velocity profile is prescribed at the jet inlet, where the jet is introduced as a pulsative stream with time-varying velocity in sinusoidal form, with periods of τ_j = 5 s, 10 s, and 20 s. The velocity of the jet stream can be calculated:

$$V_j = V_{j,max} \sin(2\pi f t) \tag{5}$$

where V_j refers to the instantaneous velocity of the jet stream, while $V_{j,max}$, f, and t are the maximum jet velocity, frequency, and time, respectively. For all cases of the fourth series calculations, the velocity ratio is V_R = 3.3, corresponding to a time-averaged jet velocity of $V_{j,avg}$ =10 m/s. The $V_{j,avg}$ is calculated:

$$V_{j,max} = \frac{V_{j,avg}}{0.637} \tag{6}$$

Figure 7 shows time-dependent jet velocity profiles graphically for each period. The parameters employed in the numerical computations for periodically-time-dependent jet velocity are presented in tab. 7.

Table 8 shows the percentage areas of temperature zones for cases IV-a, IV-b, and IV-c. Accordingly, although not shown here, almost the entire inner surface of the air duct remains in the lowest temperature zone, and the percentage of dimensionless temperature zones does not change with period of jet velocity. Therefore, antibacterial coating using the jet injection method with a periodically-time-dependent jet stream velocity is not effective.

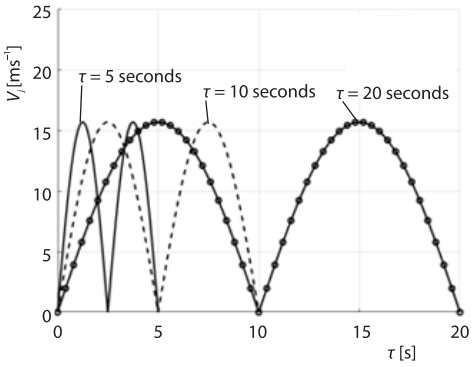

Figure 7. Sinusoidal jet inlet velocity profiles for the periods of τ_j = 5, 10, and 20 seconds

Table 7. Parameters used in the fourth series of numerical calculations

Case	T_c [K]	V_c [ms^{-1}]	T_j [K]	$V_{j,avg}$ [ms^{-1}]	τ_j [s]
IV-a	293	3.0	313	10	5
IV-b					10
IV-c					20

Table 8. Results related to the fourth series of calculations

Case	A_I [%]	A_{II} [%]	A_{III} [%]	A_{IV} [%]	A_V [%]
IV-a	99.99	0.00	0.00	0.00	0.01
IV-b	99.99	0.00	0.00	0.00	0.01
IV-c	99.99	0.00	0.00	0.00	0.01

Conclusions

The effects of the nozzle configuration, jet flow injection angle, jet-to-cross-flow velocity ratio, and periodically-time-dependent jet inlet velocity on the interaction between jet

stream and cross-flow are numerically investigated, to assess the effectiveness of the jet injection method for antibacterial coating of ventilation ducts. The results of the numerical calculations are as follows.

- The configuration with one pair of nozzles on both the bottom and top surfaces provides the most optimal temperature distribution. The existence of the opposite jets and their interaction enhances the distribution of the passive scalar, in this case temperature.
- Using the optimal geometrical model, seven different jet injection angles are studied, and angles close to 90° are found to yield better performance. For the injection angles far below or above 90°, interaction between the opposite jet streams weakens since the vertical component of jets' momentum is smaller, which causes the passive agent carried by the jet not to be transferred effectively toward the wall.
- For velocity ratios less than 3.3, a large portion of the surface area remains in low temperature zones. It is observed that the percentage areas of high temperature zones increases with the velocity ratio, which indicates an increase in the effectiveness of the coating.
- Almost the whole inner surface of the air duct remains in the lowest temperature zone, and the percentage of dimensionless temperature zones almost does not vary with the period of the jet velocity, which shows that coating employing a time-dependent jet stream velocity is ineffective.
- The key assumption of this study is that the motion of particles dispersed in an antibacterial solution is modeled as advection of a passive scalar, *i.e.*, temperature, allowing for a single-phase flow solution. Accordingly, the effectiveness of the coating is evaluated by the temperature distribution on the inner surfaces of the duct, which depends on the mixing process of the jet and cross-flow, which are at different temperatures. As a future study, comparison of the present results with those of numerical calculations which model particle motion (*e.g.*, the discrete phase model, Eulerian spray model) would provide further insight into the jet injection coating method proposed here.

Acknowledgment

This work was supported by Istanbul Aydin University and Makroteknik Inc. under a project titled *Coating Ventilation Ducts Using Jet Injection Method*.

Nomenclature

A – percentage area, [%]
D_ω – cross-diffusion modification term, [kgm^{-1}s^{-3}]
f – frequency, [s^{-1}]
G_k – turbulence kinetic energy production, [kgm^{-1}s^{-3}]
G_ω – turbulence specific dissipation rate production, [kgm^{-1}s^{-3}]
T – temperature, [K]
t – time, [s]
u_τ – shear velocity, [ms^{-1}]
V – velocity, [ms^{-1}]
V_R – velocity ratio, [–]
Y_k – turbulence kinetic energy dissipation rate, [kgm^{-1}s^{-3}]
Y_ω – turbulence kinetic energy dissipation rate, [kgm^{-1}s^{-3}]
y^+ – dimensionless distance from the wall, [–]

Greek symbols

α_j – jet injection angle, [°]
Γ_k – effective diffusivity for turbulence kinetic energy, [kgm^{-1}s^{-}]
Γ_ω – effective diffusivity for turbulence specific dissipation rate, [kgm^{-1}s^{-}]
θ – dimensionless temperature, [–]
μ – dynamic viscosity, [kgm^{-1}s^{-1}]
τ – period, [s]
ω – specific turbulence dissipation rate, [s^{-1}]

Subscripts

avg – average
c – cross-flow
i – a selected node in the computational domain
j – jet flow
max – maximum

References

[1] Ahmad, I., *et al*., Effectiveness of HVAC Duct Cleaning Procedures in Improving Indoor Air Quality, *Environmental Monitoring and Assessment*, *72* (2001), 3, pp. 265-276
[2] Szappanyos, B. J., Eckerman, R. M., Method of and Means for Controlling Mold Spores in Air-Handling Systems, US Patent No: 3 591 328, 1971
[3] ***NAIMA, Cleaning Fibrous Glass Insulated Air Duct Systems: Recommended Practice, 2007
[4] Wang, Y., *et al*., Particle Dispersion in Turbulent, Square Open Duct Flows of High Reynolds Number, *Powder Technol*., *354* (2019), Sept., pp. 92-107
[5] Sheriff, S. A., Pletcher, R. H., Measurements of the Flow and Turbulence Characteristics of Round Jets in Crossflow, *Journal Fluids Eng*., *111* (1989), 2, pp. 165-171
[6] Meyer, K. E., *et al*., Flow Mapping of a Jet in Crossflow with Stereoscopic PIV, *Journal Vis*., *5* (2002), 3, pp. 225-231
[7] Ozcan, O., Larsen, P. S., A Laser Doppler Anemometry Study of a Turbulent Jet in Crossflow, *AIAA J*., *41* (2003), 8, pp. 1614-1616
[8] Meyer, K. E., *et al*., A Turbulent Jet in Crossflow Analysed with Proper Orthogonal Decomposition, *Journal Fluid Mech*., *583* (2007), July, pp. 199-227
[9] Kamotani, Y., Greber, I., Experiments on a Turbulent Jet in a Cross-Flow, *AIAA J*., *10* (1974), 11, pp. 425-1429
[10] Smith, S. H., Mungal, M. G., Mixing, Structure and Scaling of the Jet in Crossflow, *Journal Fluid Mech*., *357* (1998), Feb., pp. 83-122
[11] Ryan, K. J., *et al*., Turbulent Scalar Mixing in a Skewed Jet in Crossflow: Experiments and Modelling, *Flow, Turbul. Combust*., *98* (2017), Nov., pp. 781-801
[12] Ivanova, E. M., *et al*., A Numerical Study on the Turbulent Schmidt Numbers in a Jet in Crossflow, *Journal Eng. Gas Turbines Power*, *135* (2013), 1, 011505
[13] Galeazzo, F. C. C., *et al*., Measurement and Simulation of Turbulent Mixing in a Jet in Crossflow, *Journal Eng. Gas Turbines Power*, *133* (2011), 6, 061504
[14] Karvinen, A., Ahlstedt, H., Comparison of Turbulence Models in Case of Jet in Crossflow Using Commercial CFD Code, Engineering Turbulence Modelling and Experiments 6, *Proceedings*, ERCOFTAC International Symposium on Engineering Turbulence Modelling and Measurements – ETMM6, Sardinia, Italia, 2005, pp. 399-408
[15] Demuren, A. O., Characteristics of 3-D Turbulent Jets in Crossflow, *Int. J. Eng. Sci*., *31* (1993), 6, pp. 99-913
[16] Keimasi, M. R., Taeibi-Rahni, M., Numerical Simulation of Jets in a Crossflow Using Different Turbulence Models, *AIAA J*., *39* (2001), 12, pp. 2268-2277
[17] Hoda, A., Acharya, S., Predictions of a Film Coolant Jet in Crossflow with Different Turbulence Models, *Journal Turbomach*., *122* (1999), 3, pp. 558-569
[18] Kalita, K., *et al*., Prediction of Turbulent Plane Jet in Crossflow, *Numer. Heat Tr. Appl*., *41* (2002), 1, pp. 101-111
[19] Huang, W., *et al.*, Influences of the Turbulence Model and the Slot Width on the Transverse Slot Injection Flow Field in Supersonic Flows, *Acta Astronaut*., *73* (2012), Apr.-May, pp. 1-9
[20] Coletti, F., *et al*., Turbulent Transport in an Inclined Jet in Crossflow, *Int. J. Heat Fluid-Flow*, *43* (2013), Oct., pp. 149-160
[21] Herrmann, M., Detailed Numerical Simulations of the Primary Atomization of a Turbulent Liquid Jet in Crossflow, *Journal Eng. Gas Turb. Power, 132* (2010), 6, 061506
[22] Chang, J., *et al*., Flow Characteristics of 2-D Classical and Pulsating Jet in Crossflow at Low Reynolds Number, *Case Stud. Therm. Eng*., *12* (2018), Sept., pp. 655-665
[23] Sau, R., Mahesh, K., Optimization of Pulsed Jets in Crossflow, *Journal Fluid Mech*., *653* (2010), Apr., pp. 365-390
[24] Kartaev, E. V., *et al.*, Formation of Counter Flow Jet Resulting from Impingement of Multiple Jets Radially Injected in a Crossflow, *Exp. Therm. Fluid Sci*., *68* (2015), Nov., pp. 310-321
[25] Menter, F. R., Two-Equation Eddy-Viscosity Turbulence Models For Engineering Applications, *AIAA Journal*, *32* (1994), 8, pp. 1598-1605

Paper submitted: December 30, 2022
Paper revised: March 28, 2023
Paper accepted: April 6, 2023